Receptor Actions of Synaptically Released Glutamate: The Role of Transporters on the Scale from Nanometers to Microns

Kaiyu Zheng, Annalisa Scimemi, and Dmitri A. Rusakov
Institute of Neurology, University College London, London, United Kingdom

ABSTRACT Actions of the excitatory neurotransmitter glutamate inside and outside the synaptic cleft determine the activity of neural circuits in the brain. However, to what degree local glutamate transporters affect these actions on a submicron scale remains poorly understood. Here we focus on hippocampal area CA1, a common subject of synaptic physiology studies. First, we use a two-photon excitation technique to obtain an estimate of the apparent (macroscopic) extracellular diffusion coefficient for glutamate, ~0.32 μm^2/ms. Second, we incorporate this measurement into a Monte Carlo model of the typical excitatory synapse and examine the influence of distributed glutamate transporter molecules on signal transmission. Combined with the results of whole-cell recordings, such simulations argue that, although glutamate transporters have little effect on the activation of synaptic α-amino-3-hydroxy-5-methyl-4-isoxazolepropionic acid receptors, this does not rule out the occurrence of up to several dozens of transporters inside the cleft. We further evaluate how the expression pattern of transporter molecules (on the 10–100 nm scale) affects the activation of *N*-methyl-D-aspartic acid or metabotropic glutamate receptors in the synaptic vicinity. Finally, we extend our simulations to the macroscopic scale, estimating that synaptic activity sufficient to excite principal neurons could intermittently raise extracellular glutamate to ~1 μM only at sparse (microns apart) hotspots. Greater rises of glutamate occur only when <5% of transporters are available (for instance, when an astrocyte fails). The results provide a quantitative framework for a better understanding of the relationship between glutamate transporters and glutamate receptor signaling.

INTRODUCTION

The activation of ''classical'' ionotropic receptors outside the synaptic cleft has emerged as an important mode of neural signaling (1–3). Activity-dependent extrasynaptic actions of the inhibitory neurotransmitter GABA can modulate cell excitability and neuronal gain (4–7). Less is understood about similar actions exerted by the excitatory neurotransmitter glutamate. In hippocampal area CA1, synaptically released glutamate is a rapidly taken up by high-affinity transporters expressed in abundance by astrocytes (8–12). The uptake keeps the average ambient glutamate concentration low, at ~25 nM in quiescent tissue (13). However, transporter-enriched glial membranes represent only ~13% of cell membranes in area CA1 (14) and approach only 30–40% of an average synaptic circumference (15). Indeed, synchronous and/or relatively strong afferent activation leads to significant activation of extrasynaptic glutamate receptors (16–18). The existence of neuronal (in particular intrasynaptic) glutamate uptake is a subject of debate. Although the blockade of glutamate transporters has little effect on α-amino-3-hydroxy-5-methyl-4-isoxazolepropionic acid receptor (AMPAR)-mediated synaptic currents (19,20), the amount of glutamate released inside the cleft may dwarf the numbers of local transporters, thus rendering their influence on AMPAR activation undetectable. The role of transporters in shaping the extracellular landscape of glutamate on different scales therefore remains incompletely understood.

An important determinant of extrasynaptic communication is the degree of extracellular diffusion retardation *R* relative to a free medium. The values of *R* assessed with a well-established iontophoretic technique (21) in area CA1 vary considerably, from 2.07–2.16 (22) to 2.92 (23). To measure this value in our conditions, we applied an alternative approach based on two-photon excitation of a fluorescent indicator ejected from an instantaneous point source (24). Although a related integrative-imaging approach exploiting a diffusion source (22,25) and indicator photobleaching (26,27) have previously been used for similar purposes, the main advantage of two-photon excitation is the ability to collect fluorescence exclusively from a thin focal plane. This provides a direct readout of concentration (24,28), avoiding potential errors inherent to deconvolution techniques. In addition, quasiinstantaneous point-source release deals with a small amount of the fluorescent probe, reducing concomitant effects of the residual fluorescence accumulated in the tissue (see below).

We incorporate diffusivity measurements into a Monte Carlo model of the typical synaptic environment to test the roles of unevenly distributed transporters on the activation of local AMPA, *N*-methyl-D-aspartic acid (NMDA), or metabotropic glutamate receptors by synaptically released glutamate. By extending simulations to the macroscopic

Submitted January 19, 2008, and accepted for publication August 5, 2008.

Address reprint requests to Dmitri A. Rusakov, Institute of Neurology, University College London, Queen Square, London WC1N 3BG, UK. Tel.: 44-207-8373611, ext. 4336; Fax: 44-207-2785616; E-mail: d.rusakov@ion.ucl.ac.uk.

Annalisa Scimemi's present address is National Institute of Neurological Disorders and Stroke, National Institutes of Health, Bethesda, MD.

Editor: David S. Weiss.

0006-3495/08/11/4584/13 $2.00

doi: 10.1529/biophysj.108.129874

(intersynaptic) scale, we also assess cooperative glutamate actions exerted by the quasiphysiological activity of multiple synapses.

MATERIALS AND METHODS

Electrophysiology

Transverse hippocampal slices (300 μM) were obtained from adult male Sprague-Dawley rats using a vibratome (VT1000S, Leica Microsystems, Wetzlar, Germany). The slicing solution, ice-cold and bubbled with 95% O_2/5% CO_2, contained (mM): 75 sucrose, 70 NaCl, 2 KCl, 1 NaH_2PO_4, 26.2 $NaHCO_3$, 5.6 $MgCl_2$, 0.5 $CaCl_2$, and 25 glucose, pH 7.4, 295–297 mOsm. Slices were stored in an interface chamber in a 0.5-mM $CaCl_2$, sucrose-free solution for >1 h before starting the electrophysiological recordings. The perfusion solution included (mM): 119 NaCl, 2.5 KCl, 1.3 $MgCl_2$, 2 $CaCl_2$, 26.2 $NaHCO_3$, 1 NaH_2PO_4, 22 glucose, pH 7.4, 295–297 mOsm. Whole-cell patch clamp recordings were obtained from CA1 pyramidal cells identified under differential interference contrast, using a pipette filled with (mM): 117.5 Cs-gluconate, 17.5 CsCl, 10 HEPES, 0.2 EGTA, 8 NaCl, 2 Mg-ATP, 0.3 GTP, and 5 QX314Br, pH 7.2. The series resistance was monitored throughout the experiment using a 3-mV step command and cells were rejected if this changed more than 20%. Miniature excitatory postsynaptic currents (EPSCs) were recorded from pyramidal cells voltage-clamped at −60 mV in the presence of picrotoxin (100 μM) and TTX (1 μM). To evoke single-synapse responses in CA1 pyramidal cells, we used minimal stimulation of presynaptic Schaffer collateral fibers (29), as detailed in our previous study (30). Experiments were performed at 33–35°C. Chemicals were purchased from Sigma (St. Louis, MO), except for the TTX, which was obtained from Alomone Labs (Jerusalem, Israel).

Extracellular diffusivity measured with two-photon excitation microscopy

To evaluate extracellular diffusion, we used a technique based on two-photon excitation of a small soluble fluorescence indicator diffusing from a point source (24). In essence, this method takes advantage of the fact that multiphoton excitation occurs only within a thin (~1 μm) focal layer of the illuminated tissue volume (31). This layer is normally much wider than extracellular gaps while being much thinner than the region of measurement (50–100 μm), implying that recorded fluorescence provides a direct readout of the indicator concentration profile (sampled in the focal plane) evolving in space and time.

We used a patch pipette (~1.0 μm tip diameter) filled with the water-soluble cell-impermeable indicator Alexa Fluor 350 (hydrazide, sodium salt (Molecular Probes, Eugene, OR), molecular weight (MW) 349; 0.2 mM in bath medium inside the pipette). The pipette was connected to a pressure line (PicoPump, WPI, Sarasota, FL) and lowered into the stratum radiatum, 30–50 μm beneath the surface, in a transverse hippocampal slice kept submerged in a recording chamber (Fig. 1 *A*). The chamber was part of a multiphoton microscopy installation comprised of a Radiance 2100 imaging system (BioRad-Zeiss) connected to an infrared femtosecond pulse laser MaiTai (SpectaPhysics-Newport, Mountain View, CA) (32). The indicator was excited at $\lambda_x = 790$ nm, with an average beam power under the objective of <1 mW, to ensure that no detectable photobleaching occurred (this was tested separately by recording 1–2 s line scans of Alexa fluorescence inside cells; not shown). The fluorescence profile recorded on the scale of 50–100 μm therefore reflected diffusion from a point source.

The pipette tip was brought into focus (Fig. 1 *A*, *arrow*) and the holding pressure was adjusted to eliminate any detectable leakage of the fluorescent indicator from the tip. In control trials, continuous pressure application exerted a concentric fluorescence increase, as expected from the point-source diffusion (Fig. 1, *A* and *C*). We then ejected the indicator using a 5- or 10-ms pressure pulse and recorded the time course of the fluorescence profile using a line scan (rate 500 Hz) positioned near the point of ejection (Fig. 1, *B* and *D*). Because of the limited elasticity of the pressure system, this pulse duration was required to achieve a minimal detectable ejection of the indicator from the pipette tip. Although on the timescale of recording (1–2 s), the pulse represented a quasiinstantaneous event, the noninstantaneous ejection event could expand the effective diffusion source size beyond the 1-μm-wide pipette tip (33). Indeed, 10–15 ms after the pulse onset, the fluorescence profile of Alexa near the tip appeared 4–5 μm wide (Fig. 1, *B*). To test whether this could distort the point-source approximation, we compared the classical point-source solution (see below) with a solution for a 5-μm-wide spherical source (the conservative-case scenario). Calculations showed that 200–300 ms post pulse, the difference in the concentration profiles between these two cases was <3%, thus confirming the validity of the point-source approach in our conditions. In separate experiments, we also applied pressure pulses in a rapidly moving bath medium (mimicking quasiinstantaneous diffusion), which confirmed that the fluorescent ejection flux ceases completely in several milliseconds post pulse.

The fluorescence profiles were therefore fitted as described earlier (24) using the classical point-source solution

$$C(r,t) = \frac{Q}{8(\pi D t)^{3/2}} \exp\left(-\frac{r^2}{4Dt}\right),$$

where $C(r,t)$ is the space-time concentration profile, Q is the total amount of ejected diffusing substance (a scaling factor), and D is the diffusion coefficient. In each experimental phase, 10–20 line-scan sweeps, 30–60 s apart, were recorded and stored as a stack of 8-bit images preserving the original brightness values. An important advantage of the instantaneous point-source approach is that individual pulses are too short to have any lasting effect on the residual fluorescence in the region of interest (which might occur due to nonspecific residual binding of a proportion of the indicator molecules to cell membranes). To ensure that the residual fluorescence accumulated during multiple pulses did not affect our estimates, we also routinely subtracted the prepulse fluorescence profile from the recorded diffusion profiles.

The parameter $D_i t_i$ (equation above, index denotes an individual sampled profile) was obtained by nonlinear least-square fitting of the Gaussian fluorescence profile $I(r,t_i)$, which is proportional to the concentration profile $C(r,t_i)$, at every time point t_i (line scans at 2-ms intervals). The classical test for linear diffusion (D = const) is that the Dt_i value should increase linearly with t_i. We observed that this linearity generally holds at >100 ms (after an initial slight deviation resulting from the pressure pulse) until ~500 ms; at >500 ms post pulse, the signal/noise ratio became too low. We therefore normally sampled all fluorescence profiles between 100 and 500 ms to obtain an estimate of D. Fitting procedures were custom-written in MATLAB7 (The MathWorks, Natick, MA).

Glutamate diffusion and uptake in the microenvironment of the Schaffer collateral-CA1 pyramidal cell synapse: a Monte Carlo model

The three-dimensional structure of Schaffer collateral-CA1 pyramidal cell synapses has been documented in detail (15,34,35), and the fate of glutamate released at these synapses has been explored in several Monte Carlo models (9,36–39). The study presented here improves the accuracy of such models by adjusting the extracellular diffusivity, synaptic environment architecture, and uneven occurrence of local glutamate transporters in accordance with the available experimental data.

First, to verify that random-walk simulations faithfully reproduce microscopic interactions between glutamate molecules and receptors, we simulated responses of 20 AMPARs to instantaneous injection of glutamate in a cylindrical volume (Fig. 2 *A*), with receptor kinetics set in accordance with Jonas et al. (40). We thus simulated the experimental arrangement of outside-out patches, excised from CA1 or CA3 pyramidal cells, where glu-

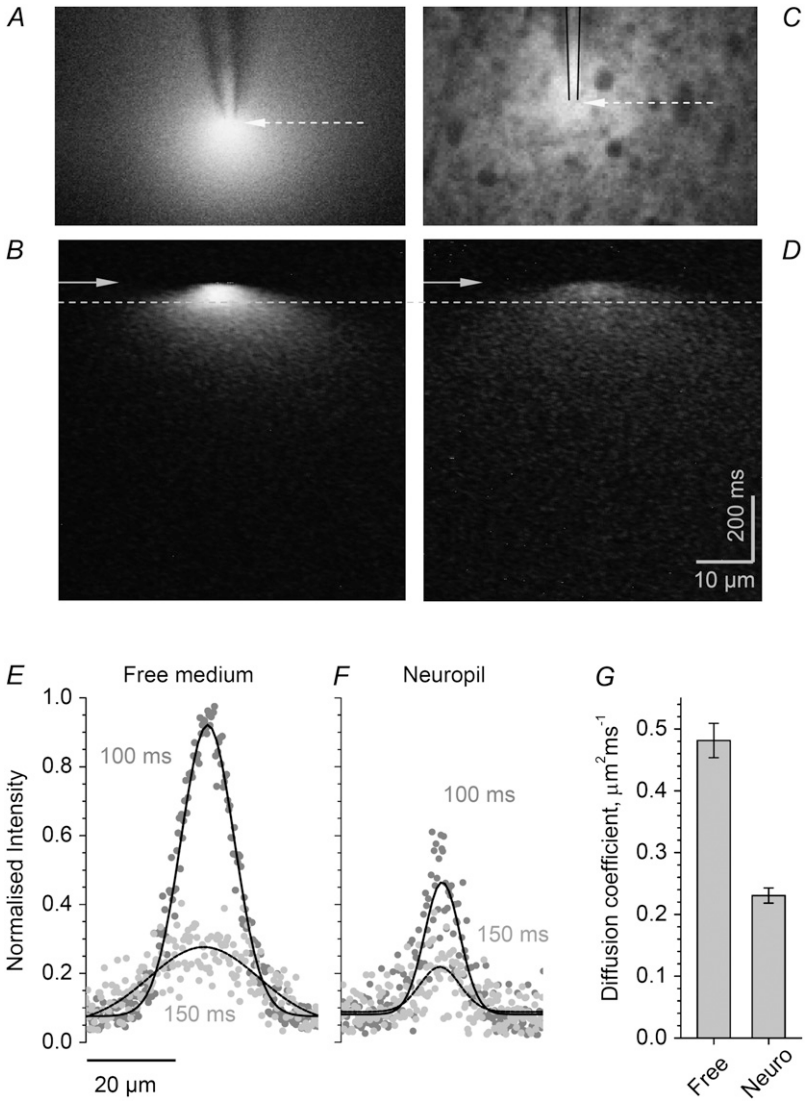

FIGURE 1 Measurements of extracellular diffusivity in the CA1 stratum radiatum using two-photon excitation imaging of point-source diffusion. (*A* and *B*) Two-photon excitation (790 nm) of Alexa Fluor 350 ejected from a patch pipette (tip diameter ~1 μm) in a free bath medium, ~50 μm above the surface of an acute hippocampal slice. (*A*) A frame scan of fluorescence averaged over 5 s during continuous pressure application; (*arrow*) line-scan position. (*B*) A line-scan image (single trial, line position shown by *dotted arrow* in *A*, depicting evolution of the fluorescence profile after a 10-ms pressure pulse (*arrow*); dotted line indicates a brightness sampling line 100 ms post pulse (see below). (*C* and *D*) Experiments similar to those in *A and B*, but in stratum radiatum of the same slice. Dark profiles represent intracellular lumen of large dendrites and cell fragments extending beyond the focal excitation plane. Notations are the same as in *A* and *B*. (*E* and *F*) Fluorescence line-scan profiles sampled at 100 ms and 150 ms post pulse in a free bath medium and inside the slice neuropil, as indicated. (*Gray* and *light gray dots*) Experimental profiles; (*black dotted lines*) the corresponding theoretical fit obtained using the instantaneous point-source diffusion equation (see Materials and Methods). Note a much slower dissipation of the fluorescence profile with time in the neuropil (*F*) compared to free medium (*E*). (*G*) The average diffusion coefficients for Alexa Fluor 350 in a free medium and in the stratum radiatum neuropil, as indicated (D_f = 0.48 ± 0.03 μm^2/ms, n = 22; and D_e = 0.23 ± 0.01 μm^2/ms, n = 37, respectively). Bars: average; error bars: mean ± SE.

tamate is applied using a rapid concentration switch (41,42). The simulated AMPAR currents at different glutamate concentrations were consistent with the experimental data (Fig. 2, *B* and *C*).

In the synaptic environment model, the presynaptic part (en-passant boutons) and the postsynaptic part (dendritic spine heads) were represented by truncated hemispheres separated by a 300-nm-wide, 20-nm-high apposition zone including a 200-nm-wide synaptic cleft (Fig. 2 *D*), consistent with the characteristic three-dimensional ultrastructure reported for these synapses (14,15,35,43). The synapse was surrounded by a system of three-dimensional 20–30-nm-wide extracellular gaps, giving an extracellular space fraction $\alpha \sim 0.15$ (22,23,44). The extracellular diffusion coefficient for glutamate (excluding space tortuosity due to cellular obstacles) was routinely set at 0.4 μm^2/ms, between the intracleft value of ~0.33 μm^2/ms estimated in electrophysiological experiments (45) and an average extracellular value of ~0.45 μm^2/ms estimated here (see Results). In baseline conditions, 80 AMPARs and 20 NMDA receptors (NMDARs) were scattered randomly within the synaptic active zone (46,47), and their kinetics were set in accordance with Jonas et al. (40) and Lester and Jahr (48), respectively. Glutamate glial transporters (EAAT1-2 type) were distributed within a spatial segment of the extrasynaptic membranes (Fig. 2 *D*) to match their average extracellular density of ~0.2 mM and a membrane surface density of 5–10 × 10^3 μm^{-2} (10), and to reflect the uneven pattern of glia surrounding these synapses (14,15).

We verified that the Monte Carlo approach simulations agreed with analytical solutions and multicompartmental algorithms operating in simpler geometries (14,39). Indeed, releasing 2000–3000 glutamate molecules in the cleft center produced synaptic currents consistent with those recorded in CA1 pyramidal cells (Fig. 2, *E* and *F*) and with the currents predicted by previous models (see above). Simulations were carried out using a dedicated 14-node PC cluster running under Linux.

From single synapses to the neuropil: matching microscopic and macroscopic models

To evaluate the dynamics of extracellular glutamate on the scale of synaptic populations, we also simulated synaptic network activity in a 40-μm-wide cube of neuropil. Although Monte Carlo modeling of free extracellular diffusion on this scale is in principle possible (49,50), the addition to the system of multiple reactions with unevenly distributed receptors would be computationally demanding (beyond a feasible scale). Furthermore, the aim of such modeling was to understand the landscape of extracellular glutamate with

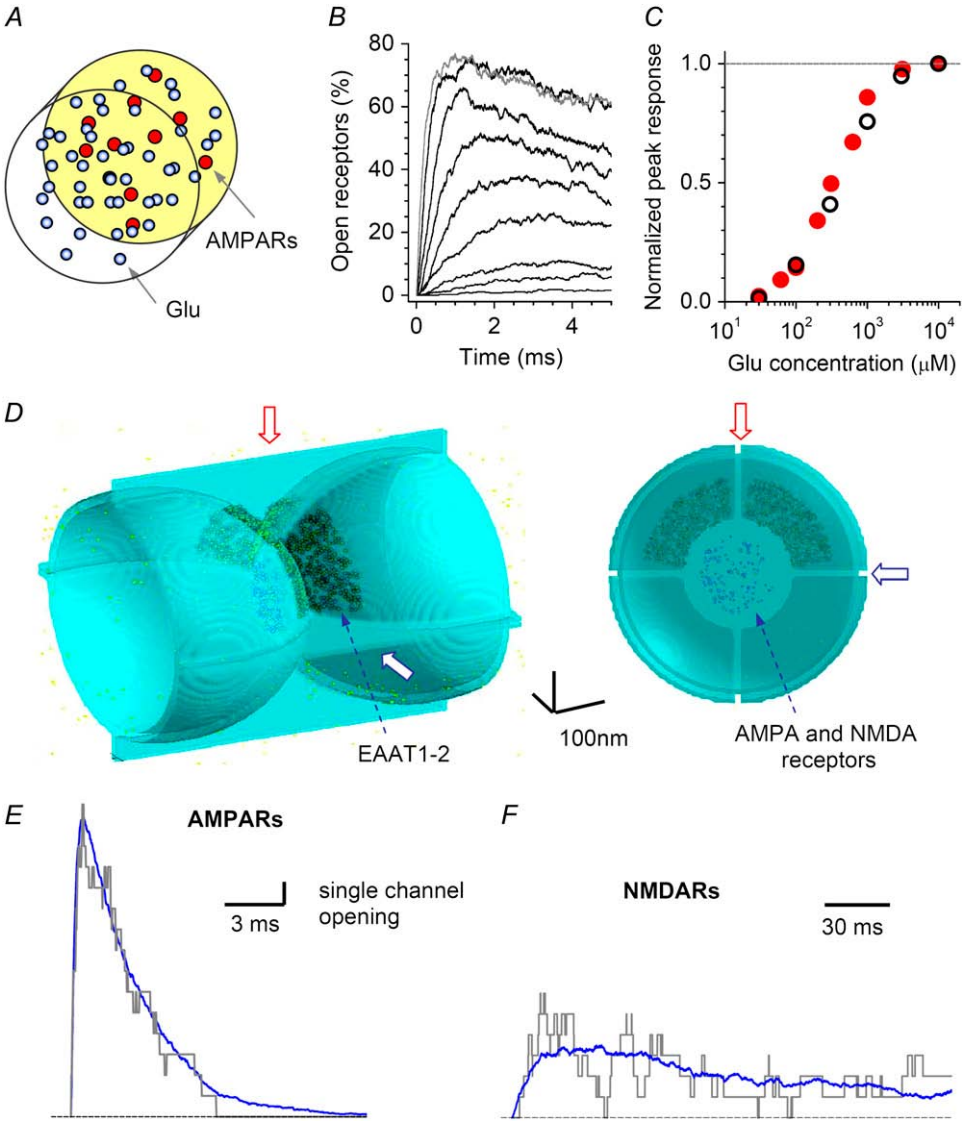

FIGURE 2 Monte Carlo model of the characteristic Schaffer collateral-CA1 pyramidal cell synapse incorporating unevenly distributed glutamate receptors and transporters. (*A–C*) A control simulation test verifying that the model reproduces faithfully the results of an experiment in which glutamate was rapidly applied to outside-out patches of CA1 or CA3 pyramidal cells (41). In a cylindrical volume (300 diameter × 300 nm height), 20 AMPARs were scattered arbitrarily over one base side, and glutamate molecules were instantaneously injected (evenly randomly, *A*) at a concentration of 30, 61, 100, 200, 301, 625, 1000, 3130, and 10000 μM, producing the corresponding current (*B*, *gray trace*, response at 10,000 μM). The summary results (*C*, *red circles*) match well with the experimental data (*open circles*) of outside-out patch experiments (41). (*D*) A diagram illustrating three-dimensional geometry of the modeled synaptic environment; (*left*) three-fourths view; (*right*) a projection of the central cross section; arrows depict some intercellular gaps; extrasynaptic membrane regions occupied by transporter molecules are seen. See Materials and Methods for details and model parameters. (*E* and *F*) The model outcome illustrating the opening time course for 80 AMPARs (*E*) and 20 NMDARs (*F*) expressed within the synaptic active zone, after release of 3000 glutamate molecules at the cleft center. (*Gray histograms* and *blue lines*) Single run and the average of 56 runs, respectively. Glutamate diffusion coefficient, 0.4 μm^2/ms, to account for extracleft (0.45 μm^2/ms) and intracleft (0.33 μm^2/ms) diffusivity (see Results).

resolution sufficient to discern effects of individual synapses (the average nearest-neighbor distance between synapses in this area is 0.5 μm (51)), rather than to trace the fate of individual glutamate molecules. We therefore modeled the neuropil on this scale as a three-dimensional porous medium (52), again with $\alpha = 0.15$ and the apparent (macroscopic) glutamate diffusion coefficient D set in accordance with the in situ measurements (see Results). Synaptic release sites for glutamate were scattered randomly, in accordance with the volume density of synapses in area CA1, $N_V = 2.0\ \mu m^{-3}$ (51). Individual sites released 3000 molecules of glutamate (see below) at an arbitrarily chosen time point.

In this macroscopic model, the space was divided into 0.25-μm-wide cubic compartments. Although this spatial resolution is sufficient to discern individual synapses (see above), averaging across individual space compartments might in principle distort the time course of extracellular glutamate in the proximity of release sites. To eliminate this source of uncertainty, we first used the Monte Carlo model (Fig. 2) to calculate the average glutamate concentration time course within virtual 0.25-μm-wide cubes that make up the simulated environment (see Fig. 6 *A*, *inset*). Next, we compared the resulting glutamate profiles with those generated by the macroscopic compartmental model in which release events were represented by a volume-average glutamate concentration jump in the synapse-containing 0.25-μm compartment. We found that the concentration time course predicted by the two models produced a reasonable match (see Fig. 6 *A*). This ensured that the macroscopic compartmental model was consistent with the microscopic events occurring in the immediate synaptic vicinity.

RESULTS

Diffusion retardation of glutamate in the extracellular space

To evaluate extracellular diffusivity, we imaged point-source diffusion of the small cell-impermeable indicator Alexa Fluor 350 (MW 349) excited in two-photon mode in a free medium (Fig. 1, *A* and *B*) and in stratum radiatum (Fig. 1, *C* and *D*) at 33–35°C. The focal-plane emission profiles were fitted, at

multiple time points postejection, by the simple theoretical curve using a single-parameter optimization (in individual scans, residual fluorescence increments due to possible nonspecific binding of the indicator were undetectable; see Materials and Methods; Fig. 1, *E* and *F*). These experiments yielded the indicator diffusion coefficients in the extracellular space and in a free medium, respectively, $D_e = 0.23 \pm 0.01\ \mu m^2/ms$ ($n = 37$) and $D_f = 0.48 \pm 0.03\ \mu m^2/ms$ ($n = 22$; Fig. 1 *G*). The average free-to-neuropil diffusion retardation factor, calculated by averaging D_f/D_e among individual slice experiments, was $R = \langle D_f/D_e \rangle = 2.66 \pm 0.43$ ($n = 19$). This corresponds to the tortuosity $\lambda = \langle (D_f/D_e)^{0.5} \rangle = 1.59$. Diffusion retardation R generally incorporates a geometric hindrance factor R_g (due to extracellular space tortuosity) and an extracellular medium viscosity factor R_v, such that $R = R_g R_v$ (53). Detailed Monte Carlo simulations of the three-dimensional neuropil represented by densely packed particles propose that $R_g = 1.4$ for the extracellular volume fraction values α of up to ~0.3 (49,50). This, together with our measurements, gives the viscosity factor $R_v = R/R_g = 1.9$.

The Alexa Fluor 350 molecules used in our measurements are only twice as heavy as glutamate molecules (MW 349 and 175, respectively), which corresponds to only a ~26% difference in their spherical hydration radii. Both species are more than an order of magnitude smaller than any intercellular gaps. Furthermore, diffusion of both Alexa Fluor 350 and a much heavier indicator Alexa Fluor 594 (MW 759) is retarded to the same relative degree by dextran solutions that mimic the extracellular medium viscosity (24). Taken together, these observations indicate that diffusion retardation of Alexa Fluor 350 in the neuropil, relative to its diffusion in a free medium, should be representative of that for glutamate.

The diffusion coefficient of glutamate (based on glutamine measurements) at 25°C in water is 0.76 $\mu m^2/ms$ (54). The viscosity of a standard physiological solution measured at 22–24°C using a falling ball viscometer is 1.05 mPa·s (53), whereas standard water viscosity in these conditions is ~10% lower: 0.93–0.95 mPa·s (55). This indicates that the glutamate diffusion coefficient at 22–24°C in the bath medium is ~0.68 $\mu m^2/ms$. However, NMR-based measurements of water self-diffusion show a ~26% increase between 25°C and 35°C (56). This predicts the glutamate diffusivity value at near-physiological temperature of $D_f = 0.68 \times 1.26 = 0.86\ \mu m^2/ms$. Our measurements (Fig. 1) suggest therefore that the average macroscopic extracellular diffusivity of glutamate in the stratum radiatum neuropil is $D_f/R = 0.32\ \mu m^2/ms$, whereas its average diffusivity in the interstitial space unhindered by cell obstacles will depend on the viscosity factor R_v only, thus yielding $D_f/R_v = 0.45\ \mu m^2/ms$.

Steady-state equilibrium of glutamate release and uptake: high safety factor

In the hippocampal neuropil, glial glutamate transporters are thought to provide >95% of glutamate uptake (11). With an average equivalent extracellular concentration $T = 0.2$ mM (10) and an upper limit cycling rate $k_c \sim 0.05\ ms^{-1}$ (8,57), these transporters should sustain steady-state glutamate uptake at a rate of up to $k_c T = 10\ \mu M \cdot ms^{-1}$. How does this compare with glutamate release in the course of synaptic activity? In area CA1, excitatory synapses occur at a density of $N_V \approx 2\ \mu m^{-3}$ (51,58). Classically, an action potential arriving at one of such synapses releases one, or occasionally more than one (59), synaptic vesicle with probability $P_r = 0.2$–0.5. Each release event frees $n_g = 2000$–3000 glutamate molecules (60–62) (although see Schikorski and Stevens (34)). The extracellular volume fraction α in the CA1 area is 0.13–0.20 (22,23) and the time-average axonal firing rate f of Schaffer collaterals is unlikely to exceed 100 Hz. These data suggest that the upper limit glutamate release rate, with all axons firing continuously, is in the region of $N_V \cdot P_r \cdot n_g \cdot \alpha^{-1} \cdot f \cdot N_A^{-1} \approx 2$–$5\ \mu M \cdot ms^{-1}$ (N_A is Avogadro's number).

However, it is unlikely that all synapses discharge glutamate at this rate. In fact, experiments in acute slices suggest that synchronous activation of only 0.5–1% of all excitatory synapses is sufficient to excite a CA1 principal neuron in the absence of inhibition (16,18). Because synaptic activity is unlikely to occur homogenously in space (and therefore clusters of higher-than-average synaptic activity are likely), we consider a conservative assumption that 10% of local synapses can be active at a time. This corresponds to a time-average glutamate release rate of 0.2–0.5 $\mu M \cdot ms^{-1}$. When compared to the steady-state glutamate uptake rate of 10 $\mu M \cdot ms^{-1}$ (see above), this figure suggests that synaptic activity in area CA1 occurs with a glutamate uptake safety factor of 20–50. This is consistent with experimental observations that suggest that synaptic glutamate release does not overwhelm transporters (13,63). Such space-and-time average estimates, however, may conceal the diversity of microscopic events occurring at a subsynaptic scale where the local transporter distribution is not homogenous.

Perisynaptic glutamate transporters have little influence on activation of intrasynaptic receptors

Do glutamate transporters occurring immediately outside the synaptic cleft affect receptor activation inside the cleft? Here we focused on AMPARs, which are expressed predominantly within the postsynaptic density (46,64) and mediate the bulk of excitatory response at the synapses in question. We used the detailed Monte Carlo model (Materials and Methods; Fig. 2) to determine whether varying the number of EAAT1-2 type glial transporters (10) outside the synaptic cleft influences synaptic AMPAR responses. Because such influences might in principle depend on the intracleft diffusion coefficient of glutamate (45), we explored this parameter around its predicted average value of ~0.45 $\mu m^2/ms$ (see above). The results show that extrasynaptic transporters have

little influence on AMPAR responses: varying the number of transporters scattered over the designated extrasynaptic segment from none to 1500 (Fig. 2 *D*; corresponds to an average local extracellular concentration of ~0.2 mM) results in only a <10% variation in receptor activation, irrespective of local glutamate diffusivity (Fig. 3 *A*).

Next, we tested the effect of glutamate transporters co-occurring with AMPARs inside the synaptic cleft. The existence of intrasynaptic glutamate uptake is debated, and the main candidate at hippocampal synapses is the neuronal transporter EAAT3 (9,11,65–67). Our simulations suggested that, unlike extrasynaptic transporters, only a few dozen intrasynaptic transporter molecules could reduce the activation of AMPARs that occur nearby (Fig. 3 *B*). (The effect was somewhat counterintuitive because the number of released glutamate molecules much exceeded the number of transporters; one possible explanation is that at the peak of AMPAR activation (several hundred microseconds post release), only a small proportion of released glutamate remains in the cleft.) This result leads to a prediction that glutamate uptake blockade should facilitate AMPAR-mediated responses when more than several dozens of transporters occur inside the cleft.

To test whether such facilitation would indeed occur in our conditions, we recorded AMPAR-mediated EPSCs in CA1 pyramidal cells either during miniature synaptic events (in 1 μM TTX) or in response to minimal stimulation that activates only one or very few synapses on the recorded cell (29). In both cases, the low density of active synapses should exclude any intersynaptic influence of escaping glutamate, with or without intact glutamate uptake (16,18), reflecting the conditions of the single-synapse model. Blocking glutamate uptake with 50 μM threo-beta-benzyloxyaspartate (TBOA) had no detectable effect in either case (Fig. 3, *C* and *D*), consistent with earlier observations made using other pharmacological tools (19,20). Such results argue that the number of intracleft transporters is unlikely to exceed 20–30; however, they do not rule out the presence of glutamate transport in the cleft in principle.

In addition to the AMPARs occurring inside the synaptic cleft, there are a number of perisynaptic receptors, in particular those diffusing laterally outside the synapse (68). Do local transporters affect activation of such receptors by glutamate? Our simulations showed that activation of the low-affinity AMPARs declines steeply with distance from the release site, consistent with previous reports (14,38,69),

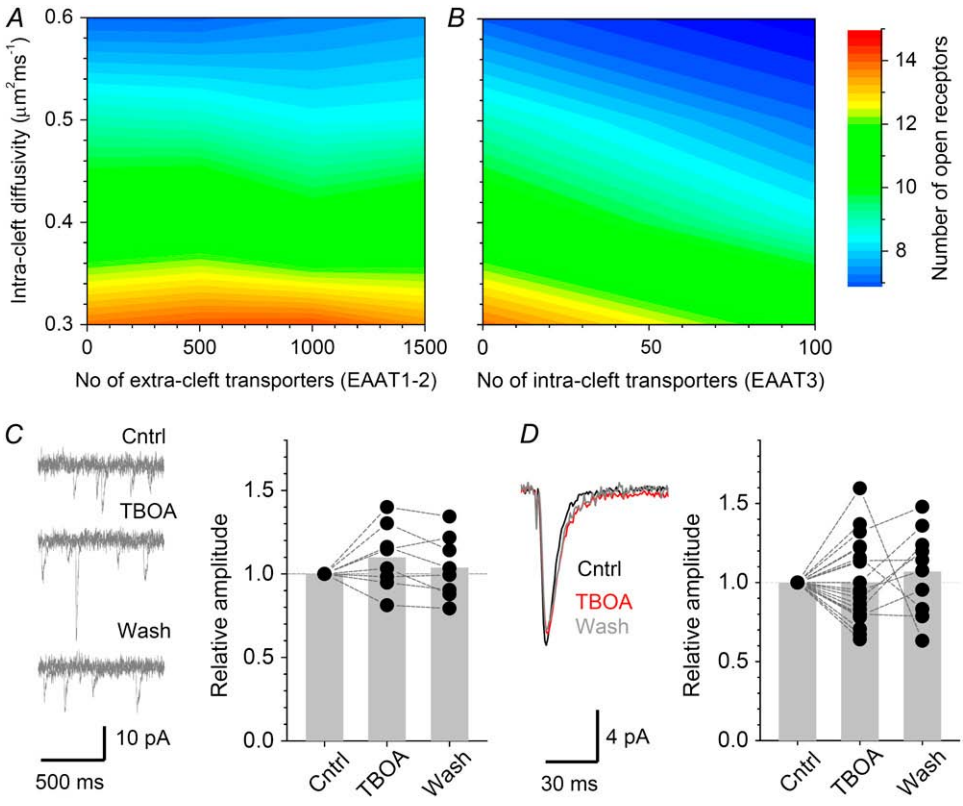

FIGURE 3 Glutamate uptake has no effect on activation of synaptic AMPARs. (*A*) The number of perisynaptic glutamate transporters (*abscissa*; see Fig. 2 *D* for transporter location; EAAT1 kinetics is adopted) has little effect on the amplitude of simulated AMPAR-mediated EPSCs (*false color scale*, the peak number of open receptors) over a plausible range of the glutamate diffusion coefficient inside the cleft (ordinate). (*B*) Intrasynaptic glutamate transporters (abscissa; EAAT3 kinetics is adopted), if present, should attenuate AMPAR-dependent EPSCs (*color scale*), depending on the transporter number, over a range of the glutamate diffusion coefficient inside the cleft (*ordinate*). (*C*) Blockade of glutamate uptake with 50 μM TBOA has no detectable effect on miniature AMPAR-dependent responses in CA1 pyramidal cells. (*Traces*) Representative examples (three consecutive traces overlapped in each panel; *Cntrl*, control; *TBOA*, application of TBOA; and *Wash*, washout). (*Plot*) Summary; (*dots*) individual cells; (*gray bars*) average values; (*dotted lines* connect data points obtained in the same cell. Average amplitude changes in TBOA and after washout relative to control are, respectively, 1.09 ± 0.06 and 1.04 ± 0.06 ($n = 9$). (*D*) Blockade of glutamate uptake with TBOA has no effect on minimal stimulation responses (AMPAR-mediated) in CA1 pyramidal cells. Traces: representative examples in control (*black*), during TBOA application (*red*), and during washout (*gray*; average of 20 traces each). (*Plot*) Summary; other notations are the same as in *C*. Average amplitude changes in TBOA and after washout relative to control are, respectively, 1.00 ± 0.06 and 1.07 ± 0.08 ($n = 21$ and $n = 11$).

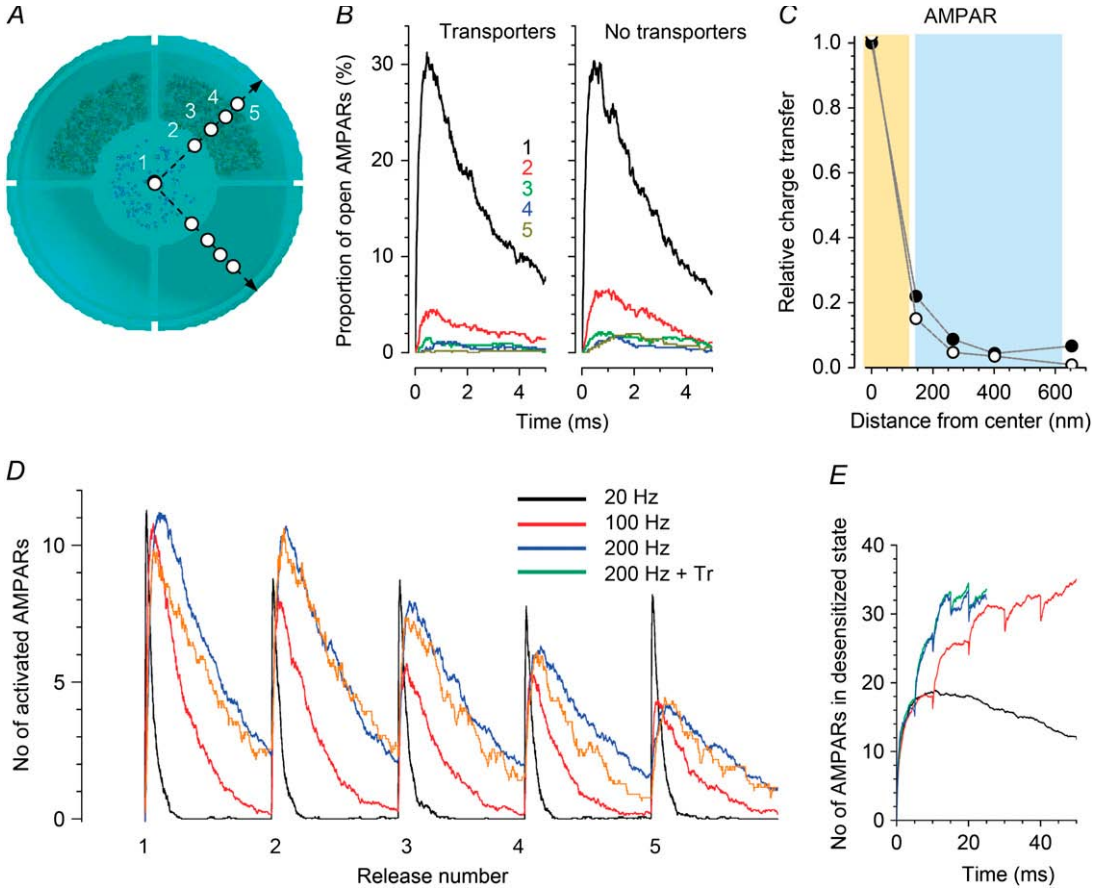

FIGURE 4 Extrasynaptic glutamate transporters have little influence on the activation of AMPARs. (*A*) Locations of the test AMPAR cluster (20 receptors; cluster positions are shown in projection by *white circles*) relative to the glutamate release site (*synaptic cleft center*), in two cases: with and without the overlapping transporter-enriched area (*upper* and *lower arrows*, respectively). Note that the projection shown masks a significant spherical curvature of the extracellular space (see Fig. 2 *D*). (*B*) Time course of the AMPAR opening (proportion of open receptors, %) at the test locations, as indicated (diagram in *A*), with and without glutamate transporters, a 28-run average. (*C*) Statistical summary: average charge transfer ($n = 28$ runs) carried by activated AMPARs at different curvilinear distances from the cleft center, relative to the charge transfer by the AMPARs located in the synaptic cleft center. (*Open* and *solid circles*) Data with and without transporters, respectively; yellow and blue shading: synaptic cleft dimensions and the spatial extent of extrasynaptic transporters (when they are present), respectively. A small stochastic error expected in Monte Carlo simulations is not shown. (*D*) Time course of AMPAR activation (number of receptors out of 80) during repetitive releases of glutamate at 20, 100, and 200 Hz, as indicated by colors; timescales are adjusted to synchronize releases. Transporters added at 200 Hz show little effect on the AMPAR activation (the effect of transporters was negligible at 20 and 100 Hz; data not shown). (*E*) Time course of AMPAR desensitization in simulation experiments depicted in *D*. Other notations are as in *D*.

with or without transporter action (Fig. 4, *A–C*). Similarly, extrasynaptic transporters have little effect on the activation of synaptic AMPARs in response to repetitive releases, when the proportion of receptors in a desensitized state gradually increases (Fig. 4, *D–E*).

Extrasynaptic transporters limit activation of nearby NMDA and metabotropic glutamate receptors depending on perisynaptic location

Some of the most plausible targets for the actions of escaped glutamate are high-affinity extrasynaptic NMDARs, particularly those containing the NR2B subunit (70–72). To determine whether spatial juxtaposition with respect to transporters, on the 10–100-nm scale, plays a part in the activation of such receptors, we placed a cluster of 20 NMDARs at different distances from the release site, exploring areas either enriched or devoid of transporters (Fig. 5 *A*; in these simulations, we assumed that the neuronal membranes were sufficiently depolarized to relieve the Mg^{2+} block of the NMDARs). Because of the unreasonably long computing time (weeks) required to simulate microscopic events for 200 ms post release in each set of conditions, we documented the NMDAR charge transfer between 0 and 20 ms post release. This parameter should faithfully represent the degree of receptor activation because the amount of glutamate remaining in the system by that time point is negligible. The results indicate that the activation of intrasynaptic NMDARs is largely insensitive to transporter actions, whereas activation of extrasynaptic NMDARs is clearly reduced when these receptors

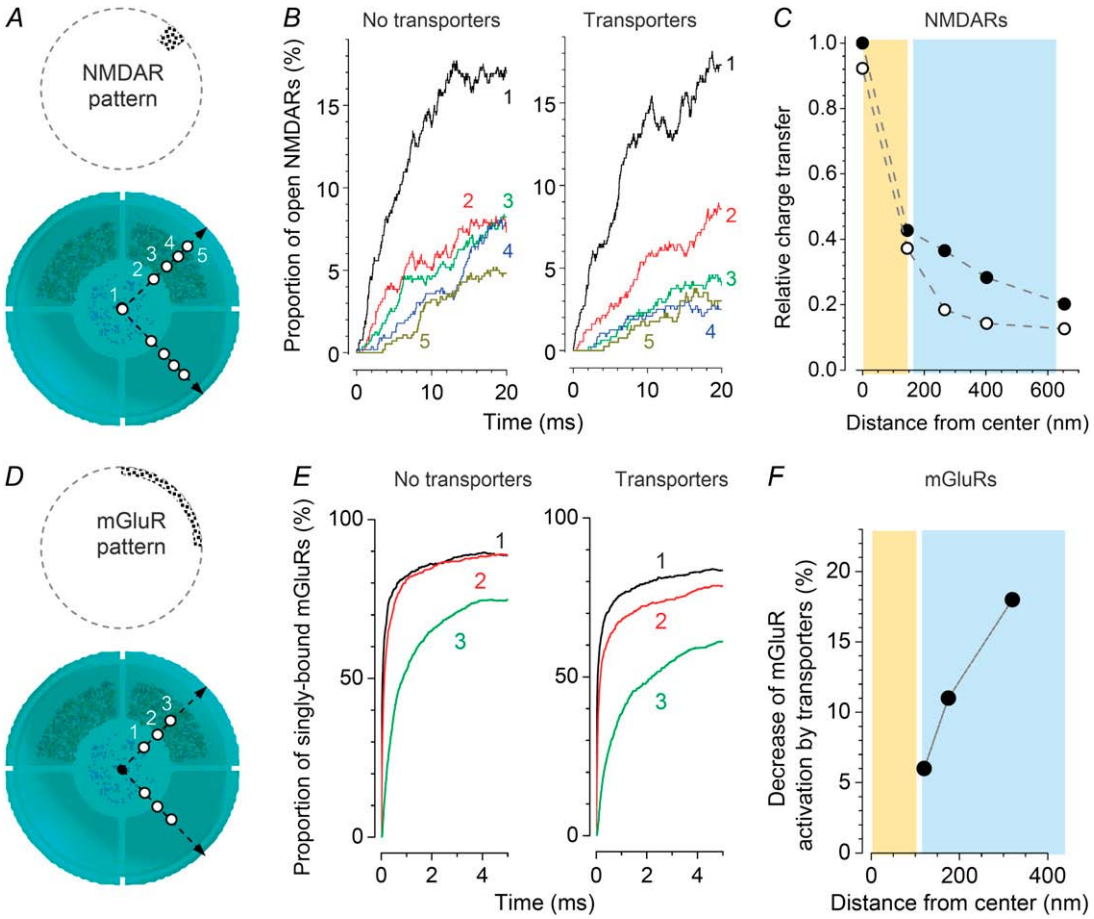

FIGURE 5 Extrasynaptic glutamate transporters reduce activation of nearby NMDARs and mGluRs by synaptically released glutamate. (*A*) Locations of the test NMDAR cluster (20 receptors; cluster positions are shown in projection by *white circles*, as in Fig. 4 *A*). (*B*) Time course of NMDAR opening (proportion of open receptors, %) at the test locations, as indicated (diagram in *A*), with and without glutamate transporters, as indicated, 28 run average. (*C*) Statistical summary of simulations shown in *B*: average charge transfer carried by activated NMDARs between 0 and 20 ms post release (value relative to the charge transfer by NMDARs located in the synaptic cleft center, with no transporters) at different curvilinear distances from the cleft center. (*Open* and *solid circles*) Data with and without transporters, respectively; (*yellow* and *blue shading*) synaptic cleft dimensions and the spatial extent of extrasynaptic transporters (when they are present), respectively. A small stochastic error expected in Monte Carlo simulations is not shown. (*D*) Locations of the test mGluR cluster (20 receptors distributed along synaptic perimeter; cluster positions are shown in projection by *white circles*, as in *A*). (*E*) Time course of mGluR activation (proportion of singly bound receptors, %). Other notations are as in *B*. (*F*) Statistical summary of simulations shown in *E*: a relative decrease of mGluR binding by glutamate in the presence of transporters at different distances from the release site. Other notations are as in *C*.

occur in the vicinity of transporters (Fig. 5, *B–D*). In general, however, the NMDAR activation level at distances of up to 600 nm from the release site remained above 10% of that inside the cleft (Fig. 5 *C*). This is somewhat higher than earlier theoretical estimates based on compartmental models, in which both glutamate and transporters were represented by the continuously distributed concentrations (14,18,37) (see Discussion).

We next asked to what degree local glutamate transporters affect activation of perisynaptic metabotropic glutamate receptors (mGluRs). Although a facilitatory effect of transporter blockade on mGluR activation has been demonstrated in electrophysiological experiments (73,74), it is not fully understood whether this reflects events on a submicron, as opposed to macroscopic, scale. Because the exact kinetics of the physiological actions exerted by mGluRs is not known, we considered the proportion of mGluRs singly bound by glutamate post release (75,76), as implemented in the General Neural Simulation System (GENESIS) computational medium (77). In our model, mGluRs were distributed either at the synaptic perimeter, in accordance with experimental observations (78,79), or farther away, maintaining the shape of a concentric ring segment (Fig. 5 *D*). Simulations indicated that the net effect of perisynaptic transporters on the activation of local mGluRs is modest (5–20%), but in relative terms increases rapidly with distance from the release site (Fig. 5, *D–F*). Because electrophysiological experiments showed substantially

greater effects of the transporter blockade (73), our results suggest that either the recorded physiological actions of mGluRs are highly supralinear with respect to receptor binding to glutamate or these receptors occur, on average, at a significant distance from glutamate release sites.

Glutamate hot-spot landscape in the extracellular space is shaped by glutamate transport

To evaluate the extrasynaptic and long-range actions of glutamate, we simulated a $(40\ \mu m)^3$ neuropil region divided into 0.25-μm space compartments. On a local scale, we confirmed that the compartmental approach faithfully represents the microscopic events occurring in the synaptic vicinity, by comparing the volume-average glutamate concentration time course obtained using the Monte Carlo model with that obtained with the compartmental model (Materials and Methods; Fig. 6 *A*). On the scale of neuropil, we distributed glutamate release sites representing individual synapses as a hard-core spatial Poisson process (uniformly random process of rigid spheres with a density of 2.0 μm^{-3} and a core radius of 300 nm) to reflect the pattern of excitatory synapses in the CA1 area (15,51,58). The model allowed us to activate arbitrarily selected synapses at arbitrary time points.

To examine the landscape of extracellular glutamate during the unevenly distributed synaptic activity, we initiated release from multiple sites within two separate active ''pools'' of synapses (spherical regions, 5 and 15 μm wide, 10 μm apart; Fig. 6 *B*). Within each pool, synaptic discharges followed a stochastic Poisson process, so that ~2% of synapses discharged randomly over a 10-ms time widow (equivalent to an average singe-synapse discharge rate of ~2 Hz). This intensity reflects experimental estimates of the (upper limit) volume-average synaptic activity sufficient to excite CA1 pyramidal cells (16,18).

Outside the active pools, synapses released glutamate at a much lower average rate, ~0.05 Hz. At the baseline level of EAAT1-2 expression in the CA1 neuropil, 0.2 mM (10), this leads to an ambient glutamate concentration of 30–50 nM, consistent with recent measurements of extracellular glutamate in area CA1 in quiescent slices (13).

Simulation snapshots in Fig. 6, *C–F*, depict extracellular glutamate profiles produced at three levels of glial glutamate transporters, corresponding to 100%, 10%, 5%, and 2.5% of

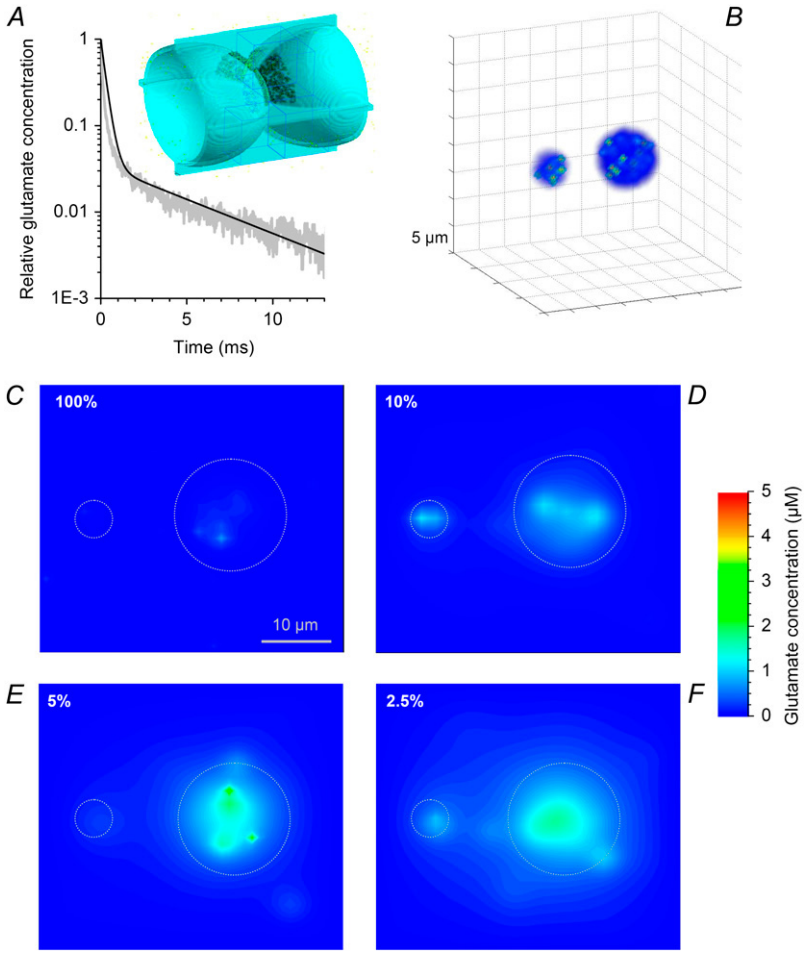

FIGURE 6 Glutamate transporters and synaptic activity shape the landscape of extracellular glutamate in the CA1 neuropil. (*A*) Matching the Monte Carlo model of the synaptic environment (Fig. 2 *D*) and the multicompartmental (macroscopic) model of the neuropil. (*Inset*) In the Monte Carlo model (geometry shown), the glutamate concentration was averaged over the 0.25-μm cubic volumes (indicated); the concentration time course was compared with that calculated using similar (equiconcentration) compartments of the macroscopic model. The number of released molecules (3000) and the average extracellular concentration of transporters (0.2 mM) were matched. (*Plot*) Gray and black lines, glutamate concentration time course in the central 0.25-μm volume calculated using, respectively, the Monte Carlo and compartmental models. (*B*) Three-dimensional impression of the two active synaptic pools in the neuropil. Colors indicate local glutamate concentrations (see *C–F* below; see text for details). (*C–F*) Snapshots of the extracellular glutamate concentration landscape in a neuropil cross section through the centers of the two active synaptic pools (*B*) in different conditions of uptake (indicated by the percentage of the functional glutamate transporters; baseline is 0.2 mM). (*False color scale*) Concentrations. See Results for details.

the baseline EAAT1-2 expression in the CA1 neuropil (10). The results indicate that when glutamate uptake is intact, synaptic activity sufficient to excite principal cells elevates the local ambient glutamate concentration only slightly, with relatively sparse ''hot spots'' reaching ~1 μM (Fig. 6 *C*). This is consistent with detectable activation of extrasynaptic NMDARs (mainly those containing NR2B subunits) in CA1 pyramidal cells after synchronous excitation of multiple Schaffer collaterals (16,18,80). Outside the active synaptic pools, however, the ambient glutamate concentration remains virtually unaffected. Furthermore, synaptic releases appear to summate in a cooperative manner: the glutamate level within the smaller synaptic pool shows almost no detectable increases even though the spatial density of release sites and the release rate are similar in both pools (Fig. 6 *C*).

A persistent increase in the ambient glutamate level above 1 μM occurs when 90% of all available transporters are switched off (Fig. 6 *D*). However, even in these conditions increases in the ambient glutamate level are still largely restricted to the pools of active synapses. It is only when 95–98% of the uptake system is impaired that glutamate released within a pool of active synapses may reach concentrations exceeding 1 μM over larger neuropil areas. In the latter case, cooperative glutamate action between active pools of synapses may occur on a scale of tens of microns (Fig. 6 *F*).

DISCUSSION

The main findings of this study are as follows: First, we measured retardation of extracellular diffusion of small molecules in hippocampal area CA1 using a concentration readout method based on two-photon imaging. Second, we combined such measurements with a Monte Carlo model and electrophysiological experiments to conclude that little effect of glutamate transport on AMPAR responses is expected irrespective of the receptor location. This contrasts with the role of extrasynaptic transporters, which reduce activation of nearby NMDARs or mGluRs. Finally, simulations of glutamate release, diffusion, and uptake on the scale of synaptic populations predict that synaptic activity sufficient to excite principal neurons leads to only modest (<1–2 μM) and sparse (microns apart) rises of ambient glutamate, within the active pool of synapses, unless the uptake systems fail catastrophically.

The updated method to measure extracellular diffusion with two-photon excitation imaging of a fluorescence point source (24) (Fig. 1) yielded an average diffusion retardation factor $R = 2.66$, which is in between the two estimates obtained earlier with an iontophoretic method (2.07–2.16 (22) and 2.92 (81)). The value of R assessed here corresponds to an average glutamate diffusion coefficient in the space between cell membranes (excluding tissue geometry) of ~0.45 μm^2/ms. Because synaptic clefts occupy only 1–2% of the extracellular space in area CA1 (82), this estimate applies predominantly to the extrasynaptic extracellular compartment. Electrophysiological experiments in cerebellar synapses suggest a lower diffusivity value inside the synaptic cleft: ~0.33 μm^2/ms (45). This disparity indicates that synaptic clefts are packed with macromolecular obstacles that exert substantial steric hindrance to the diffusing neurotransmitter molecules, consistent with recent electron microscopy evidence (83).

Detailed Monte Carlo simulations of the three-dimensional synaptic environment (Fig. 2) suggest that perisynaptic glutamate transporters have little influence on the activation of intrasynaptic AMPARs, even when their numbers are comparable to those of released glutamate molecules (Fig. 3 *A*). At the same time, only a few dozen transporters distributed quasirandomly inside the synaptic cleft should attenuate activation of co-occurring AMPARs (Fig. 3 *B*). Although this observation appears somewhat counterintuitive, we note that only a small proportion of 3000 released glutamate molecules are likely to remain in the cleft when AMPARs are at the peak of their doubly bound occupancy. When the high-affinity transporters occur nearby, they may successfully compete with AMPARs for glutamate binding. Consistent with the previous observation, our experiments show that neither miniature nor minimal-stimulation-induced (single-fiber) AMPAR-mediated EPSCs in CA1 pyramidal cells are affected by glutamate transporter blockade (Fig. 3, *C* and *D*). This result suggests that the number of glutamate transporters co-occurring with AMPARs within synaptic clefts is, if anything, small (<20–30).

Outside the cleft, activation of extrasynaptic NMDARs is substantially reduced if they share their spatial domain with glutamate transporters but could be significant if no transporters are expressed in their immediate vicinity (Fig. 5, *A–C*). This result provides a quantitative reference for evaluating the extent of extra- and/or intersynaptic signaling in the hippocampus, an issue that remains a subject of debate (18,37). The simulations presented here also predict a somewhat higher level of activation for NMDARs occurring in the transporter vicinity than previously observed in comparable conditions (14,37,51). Again, one plausible explanation is that the previous models dealt with continuous concentrations rather than with individual molecular events. In addition, glutamate transporters in the approach presented here are accumulated within a restricted area (a fragment of the glial membrane), in accordance with experimental observations, rather than distributed homogenously at a lower density. These two factors might increase the probability that diffusing glutamate molecules encounter an NMDAR before being bound to a transporter molecule. Our data also suggest that the effect of transporters on mGluR binding by glutamate increases rapidly with the distance to the release site (Fig. 5, *D–F*). This may relate the reported substantial effects of transporter blockade on mGluR responses in Purkinje cells (73) to a relatively large, rather than small, average distance between activated mGluRs and glutamate release sites. In

summary, our observations suggest that juxtaposition of receptors and transporters has a complex effect on receptor activation, which could be masked by volume averaging.

It has long been understood that the extracellular glutamate level on a macroscopic scale is determined by the number/density of available transporters. Our data provide quantitative insights into the microscopic features of the glutamate landscape shaped by the activity of multiple synapses. Although sustained synaptic activity is likely to produce sparse, relatively small (up to 1–2 μM) local increases in the ambient glutamate level, such increases do not spread appreciably outside the pool of active synapse (Fig. 6 *C*). Only when >90% of glutamate transport fails do longer-range gradients of extracellular glutamate emerge (Fig. 6, *D–F*). Again, this provides a quantitative reference for the observation that activation of extrasynaptic glutamate receptors is dramatically reduced in areas enriched in transporters (73). A striking demonstration of this principle can be found in the hypothalamic supraoptic nucleus, where the withdrawal of transporter-enriched glial processes is associated with long-range actions of synaptically released glutamate (84).

The results presented here help to elucidate the extent of intersynaptic cross talk via escaped glutamate. Intriguingly, individual astrocytes, which are responsible for the bulk of glutamate uptake in the hippocampus (11), occupy separate neuropil domains, each filling a volume of $\sim 9 \times 10^4$ μm^3 while overlapping by only 3–10% with neighboring astrocytes (85,86). This suggests that the failure of a single astrocyte could impair glutamate removal in the vicinity of $\sim 1.8 \times 10^5$ synapses. Because an individual CA1 pyramidal cell hosts $5–10 \times 10^3$ synapses (87), such glial impairment may thus affect synaptic inputs to hundreds of principal cells. This prediction is significant in the light of recent findings showing that Ca^{2+} signaling in a single astrocyte can alter synaptic transmission properties in its vicinity (88).

The authors thank Dimitri Kullmann, Leonid Savtchenko, and Kirill Volynski for valuable comments.

This work was supported by the Wellcome Trust, Medical Research Council (UK), European Union (PROMEMORIA 512012), and Human Frontier Science Program.

REFERENCES

1. Sah, P., S. Hestrin, and R. A. Nicoll. 1989. Tonic activation of NMDA receptros by ambient glutamate enhances excitability of neurons. *Science*. 246:815–818.
2. Kamermans, M., and F. Werblin. 1992. GABA-mediated positive autofeedback loop controls horizontal cell kinetics in tiger salamander retina. *J. Neurosci.* 12:2451–2463.
3. Eghbali, M., J. P. Curmi, B. Birnir, and P. W. Gage. 1997. Hippocampal GABA(A) channel conductance increased by diazepam. *Nature*. 388:71–75.
4. Mitchell, S. J., and R. A. Silver. 2003. Shunting inhibition modulates neuronal gain during synaptic excitation. *Neuron*. 38:433–435.
5. Semyanov, A., M. C. Walker, D. M. Kullmann, and R. A. Silver. 2004. Tonically active GABA A receptors: modulating gain and maintaining the tone. *Trends Neurosci.* 27:262–269.
6. Cavelier, P., M. Hamann, D. Rossi, P. Mobbs, and D. Attwell. 2005. Tonic excitation and inhibition of neurons: ambient transmitter sources and computational consequences. *Prog. Biophys. Mol. Biol.* 87:3–16.
7. Farrant, M., and Z. Nusser. 2005. Variations on an inhibitory theme: phasic and tonic activation of GABA(A) receptors. *Nat. Rev. Neurosci.* 6:215–229.
8. Bergles, D. E., and C. E. Jahr. 1998. Glial contribution to glutamate uptake at Schaffer collateral- commissural synapses in the hippocampus. *J. Neurosci.* 18:7709–7716.
9. Diamond, J. S. 2001. Neuronal glutamate transporters limit activation of NMDA receptors by neurotransmitter spillover on CA1 pyramidal cells. *J. Neurosci.* 21:8328–8338.
10. Lehre, K. P., and N. C. Danbolt. 1998. The number of glutamate transporter subtype molecules at glutamatergic synapses: chemical and stereological quantification in young adult rat brain. *J. Neurosci.* 18:8751–8757.
11. Danbolt, N. C. 2001. Glutamate uptake. *Prog. Neurobiol.* 65:1–105.
12. Huang, Y. H., and D. E. Bergles. 2004. Glutamate transporters bring competition to the synapse. *Curr. Opin. Neurobiol.* 14:346–352.
13. Herman, M. A., and C. E. Jahr. 2007. Extracellular glutamate concentration in hippocampal slice. *J. Neurosci.* 27:9736–9741.
14. Lehre, K. P., and D. A. Rusakov. 2002. Asymmetry of glia near central synapses favors presynaptically directed glutamate escape. *Biophys. J.* 83:125–134.
15. Ventura, R., and K. M. Harris. 1999. Three-dimensional relationships between hippocampal synapses and astrocytes. *J. Neurosci.* 19:6897–6906.
16. Arnth-Jensen, N., D. Jabaudon, and M. Scanziani. 2002. Cooperation between independent hippocampal synapses is controlled by glutamate uptake. *Nat. Neurosci.* 5:325–331.
17. Lozovaya, N. A., S. E. Grebenyuk, T. Tsintsadze, B. Feng, D. T. Monaghan, and O. A. Krishtal. 2004. Extrasynaptic NR2B and NR2D subunits of NMDA receptors shape 'superslow' afterburst EPSC in rat hippocampus. *J. Physiol.* 558:451–463.
18. Scimemi, A., A. Fine, D. M. Kullmann, and D. A. Rusakov. 2004. NR2B-containing receptors mediate cross talk among hippocampal synapses. *J. Neurosci.* 24:4767–4777.
19. Sarantis, M., L. Ballerini, B. Miller, R. A. Silver, M. Edwards, and D. Attwell. 1993. Glutamate uptake from the synaptic cleft does not shape the decay of the non-NMDA component of the synaptic current. *Neuron*. 11:541–549.
20. Isaacson, J. S., and R. A. Nicoll. 1993. The uptake inhibitor L-trans-PDC enhances responses to glutamate but fails to alter the kinetics of excitatory synaptic currents in the hippocampus. *J. Neurophysiol.* 70:2187–2191.
21. Nicholson, C., and J. M. Phillips. 1981. Ion diffusion modified by tortuosity and volume fraction in the extracellular microenvironment of the rat cerebellum. *J. Physiol.* 321:225–257.
22. Hrabetova, S. 2005. Extracellular diffusion is fast and isotropic in the stratum radiatum of hippocampal CA1 region in rat brain slices. *Hippocampus*. 15:441–450.
23. McBain, C. J., S. F. Traynelis, and R. Dingledine. 1990. Regional variation of extracellular space in the hippocampus. *Science*. 249:674–677.
24. Savtchenko, L. P., and D. A. Rusakov. 2005. Extracellular diffusivity determines contribution of high-versus low-affinity receptors to neural signaling. *Neuroimage*. 25:101–111.
25. Nicholson, C., and L. Tao. 1993. Hindered diffusion of high molecular weight compounds in brain extracellular microenvironment measured with integrative optical imaging. *Biophys. J.* 65:2277–2290.
26. Binder, D. K., M. C. Papadopoulos, P. M. Haggie, and A. S. Verkman. 2004. In vivo measurement of brain extracellular space diffusion by cortical surface photobleaching. *J. Neurosci.* 24:8049–8056.

27. Papadopoulos, M. C., J. K. Kim, and A. S. Verkman. 2005. Extracellular space diffusion in central nervous system: anisotropic diffusion measured by elliptical surface photobleaching. *Biophys. J.* 89:3660–3668.
28. Brown, E. B., E. S. Wu, W. Zipfel, and W. W. Webb. 1999. Measurement of molecular diffusion in solution by multiphoton fluorescence photobleaching recovery. *Biophys. J.* 77:2837–2849.
29. Dobrunz, L. E., and C. F. Stevens. 1997. Heterogeneity of release probability, facilitation, and depletion at central synapses. *Neuron.* 18:995–1008.
30. Rusakov, D. A., and A. Fine. 2003. Extracellular Ca^{2+} depletion contributes to fast activity-dependent modulation of synaptic transmission in the brain. *Neuron.* 37:287–297.
31. Zipfel, W. R., and W. W. Webb. 2001. In vivo diffusion measurements using multiphoton excitation fluorescence photobleaching recovery and fluorescence correlation microscopy. *In* Methods in Cellular Imaging, A. Periasamy, editor. Oxford University Press, Oxford, UK. 216–235.
32. Scott, R., and D. A. Rusakov. 2006. Main determinants of presynaptic Ca^{2+} dynamics at individual mossy fiber-CA3 pyramidal cell synapses. *J. Neurosci.* 26:7071–7081.
33. Kiskin, N. I., and D. Ogden. 2002. Two-photon excitation and photolysis by pulsed laser illumination modelled by spatially non-uniform reactions with simultaneous diffusion. *Eur. Biophys. J.* 30: 571–587.
34. Schikorski, T., and C. F. Stevens. 1997. Quantitative ultrastructural analysis of hippocampal excitatory synapses. *J. Neurosci.* 17:5858–5867.
35. Shepherd, G. M. G., and K. M. Harris. 1998. Three-dimensional structure and composition of CA3 → CA1 axons in rat hippocampal slices: implications for presynaptic connectivity and compartmentalization. *J. Neurosci.* 18:8300–8310.
36. Clements, J. D. 1996. Transmitter timecourse in the synaptic cleft: its role in central synaptic function. *Trends Neurosci.* 5:163–170.
37. Franks, K. M., T. M. Bartol Jr., and T. J. Sejnowski. 2002. A Monte Carlo model reveals independent signaling at central glutamatergic synapses. *Biophys. J.* 83:2333–2348.
38. Raghavachari, S., and J. E. Lisman. 2004. Properties of quantal transmission at CA1 synapses. *J. Neurophysiol.* 92:2456–2467.
39. Savtchenko, L. P., and D. A. Rusakov. 2007. The optimal height of the synaptic cleft. *Proc. Natl. Acad. Sci. USA.* 104:1823–1828.
40. Jonas, P., G. Major, and B. Sakmann. 1993. Quantal components of unitary EPSCs at the mossy fibre synapse on CA3 pyramidal cells of rat hippocampus. *J. Physiol.* 472:615–663.
41. Jonas, P., and B. Sakmann. 1992. Glutamate receptor channels in isolated patches from CA1 and CA3 pyramidal cells of rat hippocampal slices. *J. Physiol.* 455:143–171.
42. Sylantyev, S., L. P. Savtchenko, Y. P. Niu, A. I. Ivanov, T. P. Jensen, D. M. Kullmann, M. Y. Xiao, and D. A. Rusakov. 2008. Electric fields due to synaptic currents sharpen excitatory transmission. *Science.* 319:1845–1849.
43. Harris, K. M., F. E. Jensen, and B. Tsao. 1992. Three-dimensional structure of dendritic spines and synapses in rat hippocampus (CA1) at postnatal day 15 and adult ages: implications for the maturation of synaptic physiology and long-term potentiation. *J. Neurosci.* 12:2685–2705.
44. Perez-Pinon, M. A., L. Tao, and C. Nicholson. 1995. Extracellular potassium, volume fraction, and tortuosity in rat hippocampal CA1, CA3, and cortical slices during ischemia. *J. Neurophysiol.* 74:565–573.
45. Nielsen, T. A., D. A. DiGregorio, and R. A. Silver. 2004. Modulation of glutamate mobility reveals the mechanism underlying slow-rising AMPAR EPSCs and the diffusion coefficient in the synaptic cleft. *Neuron.* 42:757–771.
46. Takumi, Y., V. Ramirez-Leon, P. Laake, E. Rinvik, and O. P. Ottersen. 1999. Different modes of expression of AMPA and NMDA receptors in hippocampal synapses. *Nat. Neurosci.* 2:618–624.
47. Racca, C., F. A. Stephenson, P. Streit, J. D. B. Roberts, and P. Somogyi. 2000. NMDA receptor content of synapses in stratum radiatum of the hippocampal CA1 area. *J. Neurosci.* 20:2512–2522.
48. Lester, R. A. J., and C. E. Jahr. 1992. NMDA channel behavior depends on agonist affinity. *J. Neurosci.* 12:635–643.
49. Hrabetova, S., J. Hrabe, and C. Nicholson. 2003. Dead-space microdomains hinder extracellular diffusion in rat neocortex during ischemia. *J. Neurosci.* 23:8351–8359.
50. Hrabe, J., S. Hrabetova, and K. Segeth. 2004. A model of effective diffusion and tortuosity in the extracellular space of the brain. *Biophys. J.* 87:1606–1617.
51. Rusakov, D. A., and D. M. Kullmann. 1998. Extrasynaptic glutamate diffusion in the hippocampus: ultrastructural constraints, uptake, and receptor activation. *J. Neurosci.* 18:3158–3170.
52. Nicholson, C., and M. E. Rice. 1987. Calcium diffusion in the brain cell microenvironment. *Can. J. Physiol. Pharmacol.* 65:1086–1091.
53. Rusakov, D. A., and D. M. Kullmann. 1998. Geometric and viscous components of the tortuosity of the extracellular space in the brain. *Proc. Natl. Acad. Sci. USA.* 95:8975–8980.
54. Longsworth, L. G. 1953. Diffusion measurements at 25° of aqueous solutions of amino acids, peptides and sugars. *J. Am. Chem. Soc.* 75:5705–5709.
55. Berstad, D. A., B. Knapstad, M. Lamvik, P. A. Skjølsvik, K. Tørklep, and H. A. Øye. 1988. Accurate measurements of the viscosity of water in the temperature range 19.5–25.5°C. *Physica A.* 151:246–280.
56. Holz, M., S. R. Heil, and A. Sacco. 2000. Temperature-dependent self-diffusion coefficients of water and six selected molecular liquids for calibration in accurate ^{1}H-NMR PFG measurements. *Phys. Chem. Chem. Phys.* 2:4740–4742.
57. Wadiche, J. I., and M. P. Kavanaugh. 1998. Macroscopic and microscopic properties of a cloned glutamate transporter chloride channel. *J. Neurosci.* 18:7650–7661.
58. Geinisman, Y., L. de Toledo-Morrell, F. Morrell, I. S. Persina, and M. Rossi. 1992. Structural synaptic plasticity associated with the induction of long-term potentiation is preserved in the dentate gyrus of aged rats. *Hippocampus.* 2:445–456.
59. Oertner, T. G., B. L. Sabatini, E. A. Nimchinsky, and K. Svoboda. 2002. Facilitation at single synapses probed with optical quantal analysis. *Nat. Neurosci.* 5:657–664.
60. Harris, K. M., and P. Sultan. 1995. Variation in the number, location and size of synaptic vesicles provides an anatomical basis for the nonuniform probability of release at hippocampal Ca1 synapses. *Neuropharmacology.* 34:1387–1395.
61. Zampighi, G. A., and R. S. Fisher. 1997. Polyhedral protein cages encase synaptic vesicles and participate in their attachment to the active zone. *J. Struct. Biol.* 119:347–359.
62. Takamori, S., M. Holt, K. Stenius, E. A. Lemke, M. Gronborg, D. Riedel, H. Urlaub, S. Schenck, B. Brugger, P. Ringler, S. A. Muller, B. Rammner, F. Grater, J. S. Hub, B. L. De Groot, G. Mieskes, Y. Moriyama, J. Klingauf, H. Grubmuller, J. Heuser, F. Wieland, and R. Jahn. 2006. Molecular anatomy of a trafficking organelle. *Cell.* 127:831–846.
63. Diamond, J. S., and C. E. Jahr. 2000. Synaptically released glutamate does not overwhelm transporters on hippocampal astrocytes during high-frequency stimulation. *J. Neurophysiol.* 83:2835–2843.
64. Nusser, Z., R. Lujan, G. Laube, J. D. B. Roberts, E. Molnar, and P. Somogyi. 1998. Cell type and pathway dependence of synaptic AMPA receptor number and variability in the hippocampus. *Neuron.* 21:545–559.
65. Furuta, A., L. J. Martin, C. L. G. Lin, M. Dykes-Hoberg, and J. D. Rothstein. 1997. Cellular and synaptic localization of the neuronal glutamate transporters excitatory amino acid transporter 3 and 4. *Neuroscience.* 81:1031–1042.
66. Jackson, M., W. Song, M. Y. Liu, L. Jin, M. Dykes-Hoberg, C. L. G. Lin, W. J. Bowers, H. J. Federoff, P. C. Sternweis, and

J. D. Rothstein. 2001. Modulation of the neuronal glutamate transporter EAAT4 by two interacting proteins. *Nature*. 410:89–93.

67. He, Y., W. G. M. Janssen, J. D. Rothstein, and J. H. Morrison. 2000. Differential synaptic localization of the glutamate transporter EAAC1 and glutamate receptor subunit GluR2 in the rat hippocampus. *J. Comp. Neurol.* 418:255–269.
68. Heine, M., L. Groc, R. Frischknecht, J. C. Beique, B. Lounis, G. Rumbaugh, R. L. Huganir, L. Cognet, and D. Choquet. 2008. Surface mobility of postsynaptic AMPARs tunes synaptic transmission. *Science*. 320:201–205.
69. Wahl, L. M., C. Pouzat, and K. J. Stratford. 1996. Monte Carlo simulation of fast excitatory synaptic transmission at a hippocampal synapse. *J. Neurophysiol.* 75:597–608.
70. Tovar, K. R., and G. L. Westbrook. 1999. The incorporation of NMDA receptors with a distinct subunit composition at nascent hippocampal synapses in vitro. *J. Neurosci.* 19:4180–4188.
71. Misra, C., S. G. Brickley, M. Farrant, and S. G. Cull-Candy. 2000. Identification of subunits contributing to synaptic and extrasynaptic NMDA receptors in Golgi cells of the rat cerebellum. *J. Physiol.* 524:147–162.
72. Prybylowski, K., Z. Y. Fu, G. Losi, L. M. Hawkins, J. H. Luo, K. Chang, R. J. Wenthold, and S. Vicini. 2002. Relationship between availability of NMDA receptor subunits and their expression at the synapse. *J. Neurosci.* 22:8902–8910.
73. Wadiche, J. I., and C. E. Jahr. 2005. Patterned expression of Purkinje cell glutamate transporters controls synaptic plasticity. *Nat. Neurosci.* 8:1329–1334.
74. Renden, R., H. Taschenberger, N. Puente, D. A. Rusakov, R. Duvoisin, L. Y. Wang, K. P. Lehre, and H. von Gersdorff. 2005. Glutamate transporter studies reveal the pruning of metabotropic glutamate receptors and absence of AMPA receptor desensitization at mature calyx of held synapses. *J. Neurosci.* 25:8482–8497.
75. Batchelor, A. M., and J. Garthwaite. 1997. Frequency detection and temporally dispersed synaptic signal association through a metabotropic glutamate receptor pathway. *Nature*. 385:74–77.
76. Attwell, D., and A. Gibb. 2005. Neuroenergetics and the kinetic design of excitatory synapses. *Nat. Rev. Neurosci.* 6:841–849.
77. Bhalla, U. S., and R. Iyengar. 1999. Emergent properties of networks of biological signaling pathways. *Science*. 283:381–387.
78. Tamaru, Y., S. Nomura, N. Mizuno, and R. Shigemoto. 2001. Distribution of metabotropic glutamate receptor mGluR3 in the mouse CNS: differential location relative to pre- and postsynaptic sites. *Neuroscience*. 106:481–503.
79. Lujan, R., J. D. B. Roberts, R. Shigemoto, H. Ohishi, and P. Somogyi. 1997. Differential plasma membrane distribution of metabotropic glutamate receptors mGluR1 alpha, mGluR2 and mGluR5, relative to neurotransmitter release sites. *J. Chem. Neuroanat.* 13:219–241.
80. Asztely, F., G. Erdemli, and D. M. Kullmann. 1997. Extrasynaptic glutamate spillover in the hippocampus: dependence on temperature and the role of active glutamate uptake. *Neuron*. 18:281–293.
81. McBain, C. J. 1994. Hippocampal inhibitory neuron activity in the elevated potassium model of epilepsy. *J. Neurophysiol.* 72:2853–2863.
82. Rusakov, D. A., E. Harrison, and M. G. Stewart. 1998. Synapses in hippocampus occupy only 1–2% of cell membranes and are spaced less than half-micron apart: a quantitative ultrastructural analysis with discussion of physiological implications. *Neuropharmacology*. 37:513–521.
83. Zuber, B., I. Nikonenko, P. Klauser, D. Muller, and J. Dubochet. 2005. The mammalian central nervous synaptic cleft contains a high density of periodically organized complexes. *Proc. Natl. Acad. Sci. USA*. 102:19192–19197.
84. Oliet, S. H. R., R. Piet, and D. A. Poulain. 2001. Control of glutamate clearance and synaptic efficacy by glial coverage of neurons. *Science*. 292:923–926.
85. Bushong, E. A., M. E. Martone, Y. Z. Jones, and M. H. Ellisman. 2002. Protoplasmic astrocytes in CA1 stratum radiatum occupy separate anatomical domains. *J. Neurosci.* 22:183–192.
86. Ogata, K., and T. Kosaka. 2002. Structural and quantitative analysis of astrocytes in the mouse hippocampus. *Neuroscience*. 113:221–233.
87. Trommald, M., V. Jensen, and P. Andersen. 1995. Analysis of dendritic spines in rat CA1 pyramidal cells intracellularly filled with a fluorescent dye. *J. Comp. Neurol.* 353:260–274.
88. Perea, G., and A. Araque. 2007. Astrocytes potentiate transmitter release at single hippocampal synapses. *Science*. 317:1083–1086.